NANO LETTERS

2006
Vol. 6, No. 9
2014−2020

Signatures of Molecular Magnetism in Single-Molecule Transport Spectroscopy

Moon-Ho Jo,[†,⊥,#] Jacob E. Grose,[‡,#] Kanhayalal Baheti,[§] Mandar M. Deshmukh,[†] Jennifer J. Sokol,[§] Evan M. Rumberger,[||] David N. Hendrickson,[||] Jeffrey R. Long,[§] Hongkun Park,*[,†] and D. C. Ralph*[,‡]

Department of Chemistry & Chemical Biology and Department of Physics, Harvard University, 12 Oxford Street, Cambridge, Massachusetts 02138, Department of Physics, Cornell University, Ithaca, New York 14853, Department of Chemistry, University of California, Berkeley, California 94720, Department of Chemistry and Biochemistry, University of California, San Diego, California 92093, and Department of Materials Science and Engineering, POSTECH, Pohang, Kyungbuk Do, Republic of Korea 790-784.

Received May 28, 2006; Revised Manuscript Received July 27, 2006

ABSTRACT

We report single-molecule-transistor measurements on devices incorporating magnetic molecules. By studying the electron-tunneling spectrum as a function of magnetic field, we are able to identify signatures of magnetic states and their associated magnetic anisotropy. A comparison of the data to simulations also suggests that sequential electron tunneling may enhance the magnetic relaxation of the magnetic molecule.

Single-molecule transistors provide a unique experimental tool for investigating the coupling between charge transport and the molecular degrees of freedom in individual molecules.[1−4] Previous studies have shown that transport spectroscopy of these structures can provide information on discrete energy excitations associated with electronic[2−4] and vibrational[1,3,4] degrees of freedom. Here we report an extension of such measurements to magnetic molecules, to study how strong intramolecular exchange forces and magnetic anisotropy in these molecules may affect the flow of tunneling electrons. Our experiments employ the prototypical single-molecule magnet $Mn_{12}O_{12}(O_2C\text{-}R)_{16}(H_2O)_4$ depicted in Figure 1a (henceforth "Mn_{12}"; here *R* represents a generic chemical functional group),[5] although as we note below our measurements suggest that this structure may not be preserved when the molecules are incorporated into our electrode geometry. Because of this uncertainty about the molecular structure, our most important conclusions are qualitative; we show how to distinguish the signals of a magnetic molecule from nonmagnetic tunneling in low-temperature current−voltage measurements, and we suggest steps that may permit future improvements in similar measurements. We find two signatures of magnetic molecular states and magnetic anisotropy: an absence of energy degeneracy between spin states at zero magnetic field (*B*) and a nonlinear evolution of energy level positions with *B*. The magnitude of zero-field splitting between spin states varies from device to device, and we interpret this as evidence for magnetic anisotropy variations upon changes in molecular geometry and environment. We do not observe hysteresis in the electron-tunneling spectrum as a function of swept magnetic field, as one might expect to find in analogy to magnetization measurements on large ensembles of Mn_{12} molecules in bulk crystals.[6−9] We discuss this absence of hysteresis in the context of predictions that magnetic excitations produced by tunneling electrons may lead to greatly enhanced magnetic relaxation.[10] We note that Heersche et al.[11] recently published an independent study of single-Mn_{12} transistors. They reported little about the magnetic-field dependence of the spectra, which is our primary focus.

Our device fabrication is similar to techniques reported previously for making single-molecule transistors.[1−3] We first produced gate electrodes by depositing 40 nm of Al and oxidizing in air at room temperature. We used electron-beam lithography and liftoff to pattern Au wires 10 nm thick and 100 nm wide, and then exposed them to oxygen plasma for 30−120 s to remove any organic contaminants. Molecules were deposited on the samples by applying dilute (∼100 μM) solutions of $Mn_{12}O_{12}(O_2CCH_3)_{16}(H_2O)_4$ ("Mn_{12}Ac") in ac-

* Corresponding authors. E-mail: ralph@ccmr.cornell.edu; Hongkun_Park@harvard.edu.
[†] Harvard University.
[‡] Cornell University.
[§] University of California, Berkeley.
[||] University of California, San Diego.
[⊥] POSTECH.
[#] These authors have contributed equally.

10.1021/nl061212i CCC: $33.50
Published on Web 08/12/2006

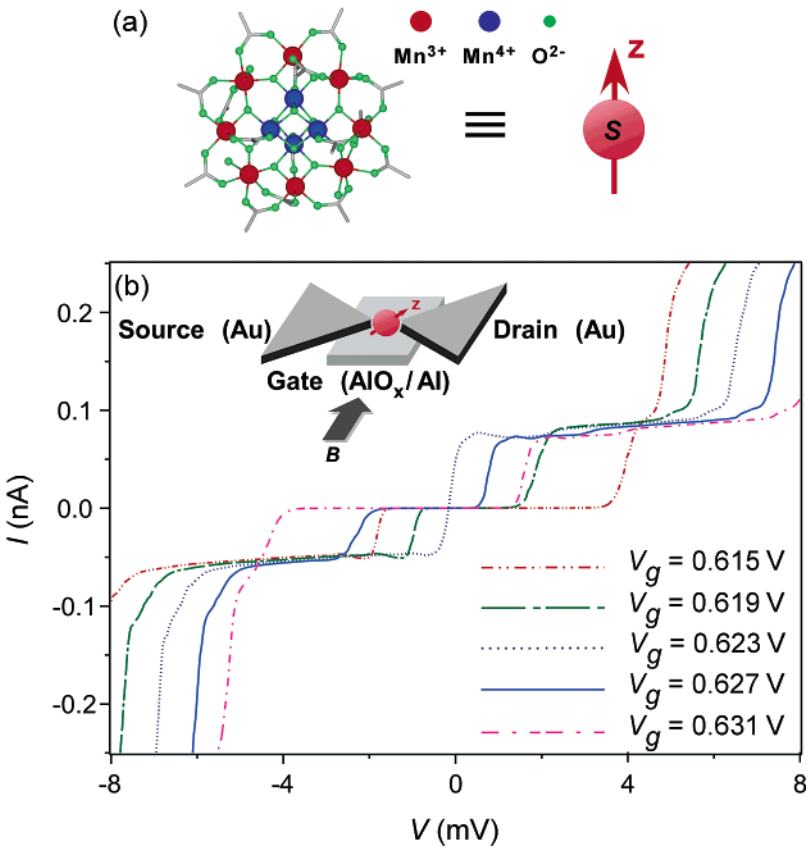

Figure 1. (a) Schematic diagram of a Mn_{12} molecule. (b) Current−voltage ($I-V$) curves at selected values of gate voltage (V_g) for a Mn_{12}Ac transistor at 300 mK. (inset) Schematic of a single-molecule transistor.

etonitrile or $Mn_{12}O_{12}(O_2CCHCl_2)_{16}(H_2O)_4$ ("Mn_{12}Cl") in methylene chloride for less than 1 min. We then created molecular-sized gaps in the gold wires using electromigration,[1] by sweeping the applied voltage (V) at a rate of approximately 30 mV/s until the wire broke (typically at 0.7−0.8 V). Some samples underwent electromigration at a temperature $T = 1.5$ K in cryogenic vacuum, and others at room temperature, with magnetic properties observed in both cases. Detailed electrical transport measurements were performed at $T \leq 300$ mK. Magnetic fields were applied parallel to the plane of the substrate; see the inset of Figure 1b. The angle of the magnetic field with respect to the magnetic anisotropy axis of the molecule is expected to vary from device to device because the adsorption geometry of Mn_{12} cannot be controlled during the deposition process.

In addition to the devices made with molecules, we conducted control experiments by preparing approximately 80 junctions from the same wafers using solvent alone. We observed simple linear tunneling $I-V$ characteristics or no measurable current in all but two of the control samples. In those two, we found Coulomb blockade characteristics; however, these devices exhibited small charging energies (<75 meV) as compared to much larger charging energies (>250 meV) in molecular devices, and could therefore be ascribed to nanoscale metal particles created by the electromigration process.[12] None of the control samples displayed any of the characteristics that we associate below with the existence of magnetic states.

We fabricated more than 70 chips of devices incorporating either Mn_{12}Ac or Mn_{12}Cl molecules, each chip containing more than 40 tunneling junctions, although not every junction on a chip was measured. Approximately 10% of these 70 chips exhibited devices with Coulomb blockade characteristics with a yield of 1−4 devices per chip (the other devices exhibited either characteristics of simple tunnel junctions or no measurable current whatsoever). In total, 16 junctions exhibiting Coulomb blockade were sufficiently stable over time for thorough investigation.

It should be noted that our measurements do not provide a means to verify that the Mn_{12} molecules remain intact through the processes of deposition and electromigration. It is possible that the molecules may lose water ligands, degrade into smaller magnetic subunits, or aggregate into larger clusters. However, the qualitative conclusions that we present about tunneling via a magnetic molecule are unaffected regardless of whether our data reflect tunneling through an intact Mn_{12} molecule or through a smaller or larger cluster with nonzero spin and magnetic anisotropy.

Figure 1b shows $I-V$ curves of a Mn_{12}Ac transistor as a function of gate voltage (V_g). The current is suppressed up to a certain threshold V, which varies linearly with V_g. This is a signature of Coulomb blockade. Outside of the blockade region, I increases in a stepwise manner with increasing V, corresponding to tunneling via discrete quantum-mechanical states.

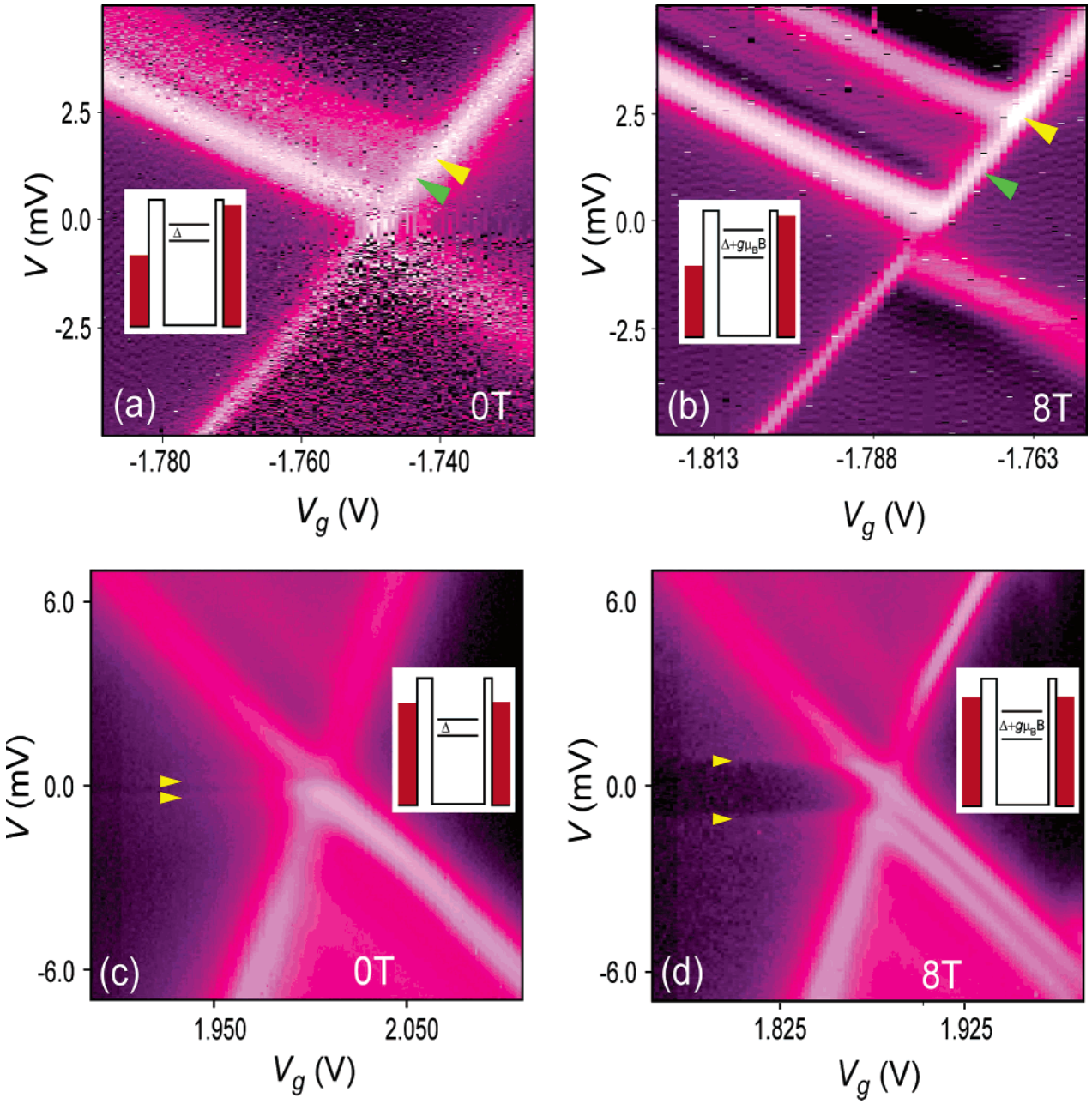

Figure 2. (a and b) dI/dV vs V and V_g for a Mn_{12}Ac transistor at $B = 0$ and 8 T. Arrows (yellow and green) indicate excited energy states. The insets depict energy diagrams for the transport features. (c and d) dI/dV vs V and V_g for a Mn_{12}Cl transistor at $B = 0$ and 8 T. Horizontal lines mark cotunneling features. The color scale in all panels varies from deep purple (10 nS) to light pink (200 nS). The scale in Figure 2 (c and d) is logarithmic.

Figure 2 shows plots of the differential conductance (dI/dV) of two devices as a function of V and V_g. In these plots, we observe crossed diagonal lines intersecting at $V = 0$ that indicate tunneling transitions between the ground energy levels of adjacent charge states. In Figure 2a, for a Mn_{12}Ac transistor, two additional peaks in dI/dV (marked with green and yellow arrows) can also be observed, corresponding to excited-state transitions with energies of ~1.1 and 1.34 meV. As a function of magnetic field (Figure 2b), neither the ground-state transition nor either of the excited-state peaks exhibits simple Zeeman splitting of degenerate spin states, in contrast to measurements in nonmagnetic quantum dot systems.[13] The existence of Zeeman splitting can be observed, in that the peak marked by the yellow arrow shifts with B to higher energy relative to the ground state, but these two transitions are not degenerate at $B = 0$. The peak marked by the green arrow does not shift with B relative to the ground state, indicating that this transition corresponds to an excited level with the same spin as the ground state, most likely due to a vibrational excitation of the molecule.[1,14,15] Parts c and d of Figure 2 show dI/dV versus V and V_g plots for a Mn_{12}Cl transistor at $B = 0$ and $B = 8$ T. Here we do not directly resolve separate ground and excited levels at $B = 0$, but instead observe inelastic cotunneling features within the left blockade region.[16] This cotunneling feature indicates the existence of an excited state with a small energy splitting

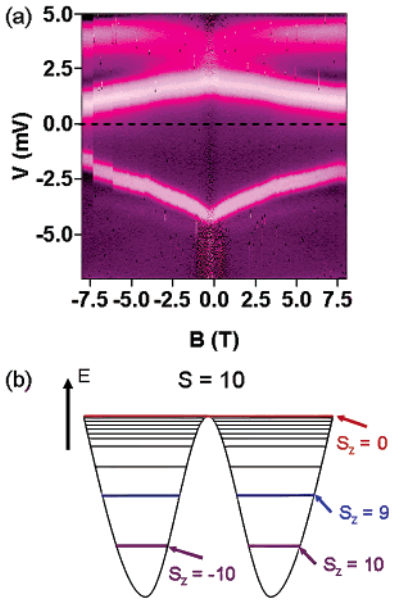

Figure 3. (a) Color plot of dI/dV vs V and B at fixed V_g for the same Mn_{12}Ac device as in Figure 2a and b. The color scale varies from deep purple (10 nS) to light pink (200 nS) (b) Energy-level diagram for the $S = 10$ multiplet in a Mn_{12} molecule.

(~0.25 meV) from the ground state. As B increases (Figure 2d), the Zeeman effect increases this splitting and the excited state becomes separately resolvable in the sequential-tunneling spectrum, so we can conclude that the splitting at $B = 0$ is between nondegenerate spin states. In total, we have observed the absence of any degenerate spin states at zero magnetic field in four different devices. We found zero-field splittings between spin states ranging from 0.25 to 1.34 meV (both extremes are represented in Figure 2).

The absence of spin-degeneracy at $B = 0$ for all states that undergo Zeeman splitting as a function of B is a signature of magnetism in a quantum system. In nonmagnetic quantum-dot systems for which the lowest-energy tunneling processes correspond to transitions from an even ($S = 0$) to an odd ($S = 1/2$) number of electrons, it is a requirement of Kramers degeneracy that the two lowest-energy tunneling transitions ($S_z = +1/2$ and $-1/2$) must exhibit simple Zeeman splitting with no zero-field splitting. To our knowledge, this is observed universally in quantum dots made from materials with exchange interactions sufficiently weak that magnetic ground states are not possible.[13] For odd-to-even transitions ($S = 1/2$ to $S = 0$) in nonmagnetic quantum dots, only one spin transition is allowed for the lowest-energy tunneling transition because of Pauli blocking so that there is no Zeeman splitting of the first tunneling state, but in this case the lowest-energy tunneling transition must shift to higher energy with increasing B.[13] In all four of the devices that we describe, the energy of the ground-state transition decreases versus B (see Figure 3a) so that this case does not apply. In quantum dots made from ferromagnetic nanoparticles, the presence of zero-field splitting has been observed previously[17,18] due to magnetic anisotropy that affects tunneling transitions between states with $S \geq 1/2$.[17,19,20] The lack of degenerate spin states at zero magnetic field in four of our devices therefore demonstrates that tunneling in these devices is occurring via magnetic states with nonzero magnetic anisotropy.[13]

In Mn_{12}, the magnetic anisotropy is associated with Jahn−Teller distortions in the octahedral coordination spheres of the eight Mn^{3+} ions, and thus it is sensitive to changes in the charge state[21] and environment of the molecule.[21−25] For example, the molecule $Mn_{12}O_{12}(O_2CCF_3)_{16}(H_2O)_4$ has been isolated in two different crystal forms, for which differences in the Jahn−Teller distortion axes around the Mn^{3+} ions give rise to different zero-field splitting parameters of $D = -0.042$ and -0.081 meV.[23] The variations in zero-field splitting observed between devices may therefore be due either to variations in the environment of each molecule as it interacts with the surface in the device or to variations in the overall molecular structure produced during the electromigration process as discussed earlier.

The other 12 devices (of 16) that we studied in detail also exhibited Zeeman splitting, but with apparent degeneracy at $B = 0$ T. We suggest that molecules in these devices may have degraded to the point of being nonmagnetic while remaining redox active. It is known that Mn_{12}Ac can degrade above 450 K,[26] and break junctions similar to ours are estimated to reach temperatures close to this value during electromigration.[27]

Figure 3a illustrates the B dependence of 1.34 meV excitation of the Mn_{12}Ac device from Figure 2a−b. Here V_g was held fixed on the more negative side of the degeneracy point and B was swept slowly from −8 T to 8 T while more rapid scans of dI/dV versus V were measured. The variations of the transition energies are continuous, symmetric around $B = 0$, and show deviations from perfect linearity. We observe no hysteresis upon reversing the direction of the field sweep.

To analyze this magnetic-field dependence, we consider the simplest model for electron tunneling via an individual magnetic molecule. We start with a model Hamiltonian that includes terms describing a uniaxial magnetic anisotropy along the z axis and the Zeeman energy corresponding to a magnetic field applied in an arbitrary direction:

$$H = D_N S_Z^2 + g\mu_B \boldsymbol{B}\cdot\boldsymbol{S} \qquad (1)$$

Here, D_N is the anisotropy constant for the multiplet with N electrons, S_Z is the z component of S, g is the electronic g-factor and μ_B is the Bohr magneton. We assume that the tunneling energies we measure in Figure 2a and b and in Figure 3a correspond to transitions between a spin S, N-electron state and a spin $S - 1/2$, $(N-1)$ electron state. For uncorrupted Mn_{12} molecules, we would expect $S = 10$, but other choices of spin states produce qualitatively similar results, as long as the difference in total spin remains 1/2. A diagram of the energy levels for eq 1 with $S = 10$ and $B = 0$ is pictured in Figure 3b. For computational simplicity, we assumed that only states in the ground-state spin multiplet of each charge state are accessible in our experiment. Similar model Hamiltonians have been considered previously in other electron-tunneling calculations.[10,17−20,28,29]

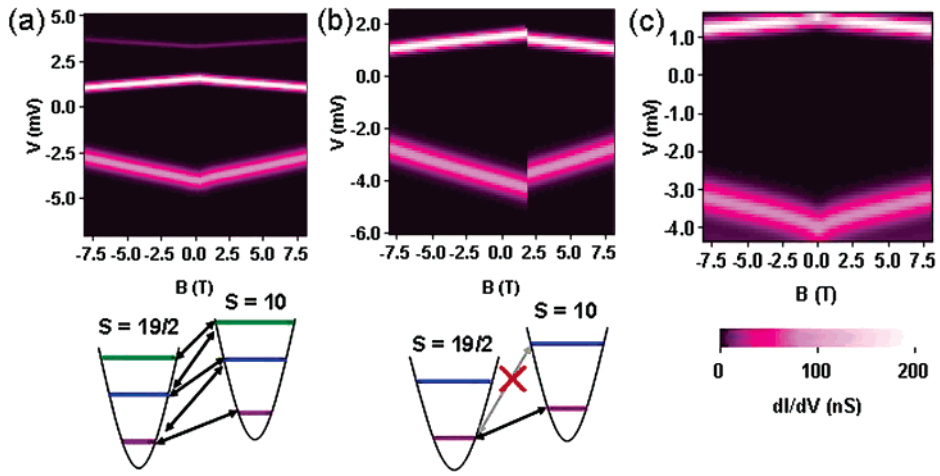

Figure 4. (a, top) There is no hysteresis as a function of B when V is swept to values large enough to allow tunneling to excited magnetic states. (a, bottom) Diagram illustrating how energetically allowed transitions provide a means to surmount the anisotropy barrier by climbing a ladder of spin states. (b) When the model includes only sequential tunneling processes (not cotunneling), a hysteretic jump in the level spectrum is predicted if V is kept sufficiently small so that tunneling to excited spin states is not allowed. (c) Curvature in the dependence of energy levels on magnetic field occurs when the strength of magnetic anisotropy is different for the two charge states. Here $D_{N-1} = -0.071$ meV and $D_N = -0.086$ meV.

From eq 1, we can identify that the magnitude of the zero field splitting observed at positive bias in Figure 3a is due to the energy difference $\Delta E = -D_N\Delta(S_Z^2)$ between the $S_z = -S$ ground state and the first excited state, $S_z = -S + 1$, for the charge state with the higher spin S. The observed energy gap in Figure 2a is 1.34 meV. Measurements on bulk crystals give $-D_N\Delta(S_z^2) = 1.08$ meV for the neutral Mn_{12} species[30] and 1.38 meV for a singly reduced Mn_{12} derivative.[21]

For more detailed comparisons to the data, we simulated the current flow through a device by determining the energy eigenstates of the molecule through numerical diagonalization of eq 1 for both the $S - 1/2$ and S multiplets and then by calculating the $I-V$ curve using a master equation approach to account for energetically allowed tunneling transitions. We included only lowest-order sequential tunneling processes. In our main simulation, we did not simply assume steady-state occupation probabilities because transitions out of metastable magnetic states may require time scales much longer than our experiment so that a true steady-state probability distribution may not be relevant experimentally. (The assumption of steady-state transition probabilities will always give nonzero weight in the true ground state and will therefore necessarily eliminate hysteresis.) We instead integrated the master equation with respect to time at each incremented value of V and/or B, until the occupation probabilities reached a quasi-steady state. We then estimated the transition rate for magnetic reversal by further integration of the master equation within the quasi-steady-state regime. We allowed occupation of states corresponding to a reversed magnetic moment only if the transition rate to these states was relevant experimentally. From the calculated distribution of occupation probabilities, we then obtained a value for I. When questions of hysteresis were not an issue, we performed the simpler alternative calculation that assumes steady-state occupation probabilities.

The results of our simulations, for parameter values chosen to mimic Figure 3a (there are too many free parameters to claim quantitative fits), are shown in Figure 4a−c. The parameters for the main simulation in Figure 4a and b are $S_{N-1} = 19/2$, $S_N = 10$, $D_N = D_{N-1} = -0.071$ meV, $g = 2.0$, a field angle of 45° with respect to the easy axis, capacitance ratios $C_{gate}/C_{source}/C_{drain} = 1{:}13{:}4$ determined from the slopes of the tunneling thresholds in Figure 2a and b, bare tunneling rates $\Gamma_{source} = 8$ GHz and $\Gamma_{drain} = 0.8$ GHz, and a magnetic field sweep rate of 0.02 T/min. The simulation in Figure 4c employs the same parameters except that we assume different anisotropy energies for the different charge states, $D_{N-1} = -0.071$ meV and $D_N = -0.086$ meV, and for Figure 4c we employ the simpler quasi-steady-state algorithm. These calculations capture many of the qualitative features of the data.

The nonlinear variation of the energy levels versus B shown in Figure 3a can be explained as a consequence of anisotropy in a magnetic molecule.[17,18] When $D_N = D_{N-1}$ (Figure 4 a and b) we find no deviation from linearity, but the sign of the curvature that is observed in Figure 3a emerges naturally if the magnetic anisotropy parameter D_N is larger for the higher-spin charge state than the smaller-spin state (Figure 4c).

The simulation (Figure 4 a and b) also reproduces naturally the number of energy levels measured in the experiment: just two at positive V and one at negative V, even though we assume large values for the total spins ($S = 10$ and 19/2 for the two charge states). The reason is that just two levels are observed at positive V is that a voltage high enough to cause tunneling to the first excited state also permits tunneling transitions higher up the ladder of spin states because transitions to higher spin states all require progressively less energy. This is consistent with our observation of only one magnetic excited state in all four devices in which we found zero-field splittings. The observation of only ground-state tunneling at negative V can be explained as a consequence of an asymmetry in the coupling of the molecule to the two electrodes, which can cause excited states to

contribute negligibly to the total current for one bias direction.[31] The excited magnetic level must be associated with the higher-spin charge state; this implies that the higher-spin state is associated with the more-positive V_g charge state in Figure 2a and b, but the more-negative V_g charge state in Figure 2c and d.

Finally, we comment on the absence of hysteresis in the electron-tunneling spectrum measured as a function of magnetic field. Magnetic measurements of macroscopic Mn_{12} crystals find low-temperature hysteresis for all field directions except those within a few degrees of the hard magnetic axis.[8,9] As illustrated in Figure 3a, however, we do not observe hysteresis in any of our devices within a magnetic field sweep range of ± 8 T, at $T \leq 300$ mK. This lack of hysteresis is also in contrast to related measurements of energy-level spectra for magnetic Co nanoparticles, with higher spin $S \approx 1000$.[17,18]

Because of the uncertainty regarding the structure of the magnetic molecules in our experiment, it is not possible to draw a definitive conclusion about why there is no hysteresis. However, one possible explanation that would be relevant to any magnetic molecule is that repeated spin transitions caused by tunneling electrons might allow the molecule to surmount the anisotropy barrier through the sequential occupation of increasingly high-energy spin states. This could allow the magnetic moment to undergo excursions between the $S_z < 0$ and $S_z > 0$ energy wells on time scales fast compared to the sweep rate of B so that there would be no abrupt changes measured in the tunneling spectrum as a function of B. For the case of magnetic nanoparticles, Waintal and Brouwer[10] predicted precisely this scenario; under certain conditions, tunneling electrons can induce magnetic relaxation despite the presence of anisotropy. More recently, Timm and Elste[32] reached similar conclusions for a single molecule magnet. This conclusion also follows from our simulations based on eq 1. We find that if, during the magnetic-field sweeps, the voltage is scanned to values sufficiently high to measure the first excited state of the higher-spin state, then there is no hysteresis (Figure 4a). This voltage is sufficiently high to enable tunneling for all allowed tunneling transitions with $\Delta S = \pm 1/2$ so that all states in the spin multiplets are accessible despite the magnetic anisotropy. Within the approximation that only lowest-order sequential tunneling processes are taken into account, the model predicts that hysteretic switching might be observed if V is kept sufficiently low that excited spin states are never populated (Figure 4b). We investigated this experimentally at selected values of V_g by applying a small constant bias V and measuring the tunneling conductance while sweeping B, but still we observed no hysteresis. Possibly this difference is due to spin excitations caused by low levels of experimental noise or by second- and higher-order cotunneling processes[16] that cause spin excitations but which are neglected in the simulation.

In conclusion, we have measured electron tunneling in devices formed by inserting Mn_{12} molecules into transistor structures. We find significant variations between devices, indicating that the sample fabrication process and the device environment may affect our molecules. Nevertheless, the devices allow us to identify signatures in the tunneling spectra by which we can distinguish tunneling via magnetic molecules from nonmagnetic tunneling: the absence of degenerate spin states at $B = 0$ and nonlinear variations of energy levels with magnetic field. We also find at most one excited magnetic level above the ground state in the tunneling spectra, in agreement with simple models. Despite the presence of the other magnetic signatures, we do not observe magnetic hysteresis. However, we point out that an absence of hysteresis is predicted by simple models of electron tunneling, because sequential tunneling transitions can populate a sequence of excited magnetic levels that surmount the anisotropy barrier and enable rapid magnetic relaxation.

Furthermore, our work provides guidance as to how these experiments may be improved to achieve transport spectroscopy on magnetic molecules with better-controlled molecular structures. One suggestion is to study single-molecule magnets that do not possess labile outer ligands and might therefore better withstand elevated temperatures that molecules might experience during the electromigration process,[27] such as tetranickel(II) complexes.[33] We also suggest additional efforts to employ molecular magnets functionalized with bridging ligands, which might enable better attachment of the molecules to electrodes after the gap between electrodes is formed so that the molecules need not be present during electromigration. Our attempts to contact Mn_{12} derivatives to electrodes after electromigration have thus far been unsuccessful. Other approaches that can be used in combination with bridging ligands, such as assembling the single-molecule magnet between a dimer of nanoparticles[34] or using carbon nanotubes as electrodes,[35] might also be possible avenues for achieving more reproducible magnetic behavior in single-molecule devices.

Acknowledgment. The work at Harvard is supported by NSF, ARO, and the Packard Foundation. The work at Cornell is supported by the NSF through the Cornell Center for Materials Research, through use of the NNIN/Cornell Nanofabrication Facility, and by ARO. The work at UC Berkeley is supported by NSF and Tyco Electronics.

References

(1) Park, H.; Park, J.; Lim, A. K. L.; Anderson, E. H.; Alivisatos, A. P.; McEuen, P. L. *Nature* **2000**, *407*, 57.
(2) Park, J.; Pasupathy, A. N.; Goldsmith, J. I.; Chang, C.; Yaish, Y.; Petta, J. R.; Rinkoski, M.; Sethna, J. P.; Abruna, H. D.; McEuen, P. L.; Ralph, D. C. *Nature* **2002**, *417*, 722.
(3) Liang, W. J.; Shores, M. P.; Bockrath, M.; Long, J. R.; Park, H. *Nature* **2002**, *417*, 725.
(4) Yu, L. H.; Natelson, D. *Nano Lett.* **2004**, *4*, 79.
(5) Gatteschi, D.; Sessoli, R. *Angew. Chem., Int. Ed.* **2003**, *42*, 268.
(6) Friedman, J. R.; Sarachik, M. P.; Tejada, J.; Ziolo, R. *Phys. Rev. Lett.* **1996**, *76*, 3830.
(7) Thomas, L.; Lionti, F.; Ballou, R.; Gatteschi, D.; Sessoli, R.; Barbara, B. *Nature* **1996**, *383*, 145.
(8) Thomas, L.; Caneschi, A.; Barbara, B. *Phys. Rev. Lett.* **1999**, *83*, 2398.
(9) Lionti, F.; Thomas, L.; Ballou, R.; Barbara, B.; Sulpice, A.; Sessoli, R.; Gatteschi, D. *J. Appl. Phys.* **1997**, *81*, 4608.
(10) Waintal, X.; Brouwer, P. W. *Phys. Rev. Lett.* **2003**, *91*, 247201.
(11) Heersche, H. B.; de Groot, Z.; Folk, J. A.; van der Zant, H. S. J.; Romeike, C.; Wegewijs, M. R.; Zobbi, L.; Barreca, D.; Tondello, E.; Cornia, A. *Phys. Rev. Lett.* **2006**, *96*, 206801.

(12) Houck, A. A.; Labaziewicz, J.; Chan, E. K.; Folk, J. A.; Chuang, I. L. *Nano Lett.* **2005**, *5*, 1685.
(13) Ralph, D. C.; Black, C. T.; Tinkham, M. *Phys. Rev. Lett.* **1995**, *74*, 3241.
(14) Pasupathy, A. N.; Park, J.; Chang, C.; Soldatov, A. V.; Lebedkin, S.; Bialczak, R. C.; Grose, J. E.; Donev, L. A. K.; Sethna, J. P.; Ralph, D. C.; McEuen, P. L. *Nano Lett.* **2005**, *5*, 203.
(15) Yu, L. H.; Keane, Z. K.; Ciszek, J. W.; Cheng, L.; Stewart, M. P.; Tour, J. M.; Natelson, D. *Phys. Rev. Lett.* **2004**, *93*, 266802.
(16) De Franceschi, S.; Sasaki, S.; Elzerman, J. M.; van der Wiel, W. G.; Tarucha, S.; Kouwenhoven, L. P. *Phys. Rev. Lett.* **2001**, *86*, 878.
(17) Gueron, S.; Deshmukh, M. M.; Myers, E. B.; Ralph, D. C. *Phys. Rev. Lett.* **1999**, *83*, 4148.
(18) Deshmukh, M. M.; Kleff, S.; Gueron, S.; Bonet, E.; Pasupathy, A. N.; von Delft, J.; Ralph, D. C. *Phys. Rev. Lett.* **2001**, *87*, 226801.
(19) Canali, C. M.; MacDonald, A. H. *Phys. Rev. Lett.* **2000**, *85*, 5623.
(20) Kleff, S.; von Delft, J.; Deshmukh, M. M.; Ralph, D. C. *Phys. Rev. B* **2001**, *64*, 220401.
(21) Aubin, S. M. J.; Sun, Z. M.; Pardi, L.; Krzystek, J.; Folting, K.; Brunel, L. C.; Rheingold, A. L.; Christou, G.; Hendrickson, D. N. *Inorg. Chem.* **1999**, *38*, 5329.
(22) Soler, M.; Wernsdorfer, W.; Sun, Z. M.; Huffman, J. C.; Hendrickson, D. N.; Christou, G. *Chem. Commun.* **2003**, *21*, 2672.
(23) Zhao, H. H.; Berlinguette, C. P.; Bacsa, J.; Prosvirin, A. V.; Bera, J. K.; Tichy, S. E.; Schelter, E. J.; Dunbar, K. R. *Inorg. Chem.* **2004**, *43*, 1359.
(24) Sessoli, R.; Tsai, H. L.; Schake, A. R.; Wang, S. Y.; Vincent, J. B.; Folting, K.; Gatteschi, D.; Christou, G.; Hendrickson, D. N. *J. Am. Chem. Soc.* **1993**, *115*, 1804.
(25) Soler, M.; Wernsdorfer, W.; Abboud, K. A.; Huffman, J. C.; Davidson, E. R.; Hendrickson, D. N.; Christou, G. *J. Am. Chem. Soc.* **2003**, *125*, 3576.
(26) Larionova, J.; Clerac, R.; Boury, B.; Le Bideau, J.; Lecren, L.; Willemin, S. *J. Mater. Chem.* **2003**, *13*, 795.
(27) Trouwborst, M. L.; van der Molen, S. J.; van Wees, B. J. *J. Appl. Phys.* **2006**, *99*, 114316.
(28) Elste, F.; Timm, C. *Phys. Rev. B* **2005**, *71*, 155403.
(29) Romeike, C.; Wegewijs, M. R.; Schoeller, H. *Phys. Rev. Lett.* **2006**, *96*, 196805.
(30) Barra, A. L.; Gatteschi, D.; Sessoli, R. *Phys. Rev. B* **1997**, *56*, 8192.
(31) Bonet, E.; Deshmukh, M. M.; Ralph, D. C. *Phys. Rev. B* **2002**, *65*, 045317.
(32) Timm, C.; Elste, F. *Phys. Rev. B* **2006**, *73*, 235304.
(33) Yang, E.-C.; Wernsdorfer, W.; Zakharov, L. N.; Karaki, Y.; Yamaguchi, A.; Isidro, R. M.; Lu, G.-D.; Wilson, S. A.; Rheingold, A. L.; Ishimoto, H.; Hendrickson, D. N. *Inorg. Chem.* **2006**, *45*, 529.
(34) Dadosh, T.; Gordin, Y.; Krahne, R.; Khivrich, I.; Mahalu, D.; Frydman, V.; Sperling, J.; Yacoby, A.; Bar-Joseph, I. *Nature* **2005**, *436*, 677.
(35) Guo, X. F.; Small, J. P.; Klare, J. E.; Wang, Y. L.; Purewal, M. S.; Tam, I. W.; Hong, B. H.; Caldwell, R.; Huang, L. M.; O'Brien, S.; Yan, J. M.; Breslow, R.; Wind, S. J.; Hone, J.; Kim, P.; Nuckolls, C. *Science* **2006**, *311*, 356.

NL061212I